Society of Medical Education & Research

2022, Volume 2, Issue 2, Page No: 57-79

ISSN: 3108-4834

Archive of International Journal of Cancer and Allied Science

GRPR-Mediated Upregulation of FAM135A Facilitates Perineural Invasion in Prostate Cancer

Sofia Maria Costa[1]*, Beatriz Nunes Lima[1], Guilherme Santos Pereira[2], Pedro Miguel Silva[2], Afonso Ribeiro Torres[3], Tiago Nuno Carvalho[3]

[1]Oncology Research Center, University of Coimbra, Coimbra, Portugal.
[2]Faculty of Medicine, University of Lisbon, Lisbon, Portugal.
[3]Institute of Biomedical Sciences Abel Salazar (ICBAS), University of Porto, Porto, Portugal.

***E-mail** ✉ s.costa.coimbra@outlook.com

Abstract

Perineural invasion (PNI) represents a clinically significant and independent indicator of metastatic risk in prostate cancer (PCa). Although gastrin-releasing peptide receptor (GRPR)–directed imaging and therapeutic approaches are currently under clinical evaluation, the contribution of GRPR signaling to PNI in PCa has not been fully elucidated. In this study, we identify Family With Sequence Similarity 135 Member A (FAM135A) as a key GRPR-activated regulator driving PNI in PCa. Transcriptomic analyses revealed enhanced neuroactive ligand–receptor interaction signaling in PNI-positive PCa tissues, with FAM135A emerging as the most prominent marker associated with this phenotype. Functional investigations using an in vitro co-culture system incorporating AR-positive (LNCaP) and AR-negative (DU145 and PC3) PCa cell lines demonstrated that suppression of FAM135A markedly reduced malignant behavior and nerve-directed invasion. Consistently, in a PCa sciatic nerve invasion mouse model, inhibition of FAM135A restrained tumor progression and significantly improved motor performance. At the subcellular level, FAM135A was predominantly localized within the nucleus, with its nuclear import dependent on the cytoplasmic–nuclear transport protein RAN. Integrated RNA-Seq and ChIP-Seq analyses further identified Teneurin Transmembrane Protein 3 (TENM3) as a direct transcriptional target of nuclear FAM135A, and TENM3 proved to be essential for FAM135A-mediated cancer–nerve interactions. Importantly, FAM135A expression was shown to be induced by gastrin-releasing peptide (GRP) through GRPR activation, while pharmacological inhibition of GRPR suppressed FAM135A expression via MED15-dependent mechanisms. Collectively, these findings establish FAM135A as a central oncodriver and potential biomarker of PNI in PCa and suggest a novel therapeutic avenue targeting tumor innervation in prostate cancer.

Keywords: FAM135A, Prostate cancer, Perineural invasion, GRPR-mediated

Introduction

Prostate cancer (PCa) remains one of the most prevalent malignancies worldwide and accounts for approximately 11% of cancer-related deaths among men [1]. Although surgical management and radiotherapy have markedly improved outcomes in patients with localized disease, nearly one-third of individuals ultimately develop disease recurrence and distant metastases, with reported 5-year survival rates declining to 30–40% in these advanced settings [2]. Androgen deprivation therapy (ADT) continues to represent the therapeutic backbone for PCa management [3]; however, the inevitable development of castration-resistant prostate cancer (CRPC) underscores the ability of tumor cells to sustain growth under low-androgen conditions [4]. These clinical challenges highlight the urgent need to better understand the molecular and cellular mechanisms that drive PCa progression in hypo-androgenic environments.

Accumulating evidence demonstrates that bidirectional communication between the nervous system and cancer

Access this article online https://smerpub.com/

Received: 05 May 2022; **Accepted:** 12 August 2022

How to cite this: Costa SM, Lima BN, Pereira GS, Silva PM, Torres AR. GRPR-Mediated Upregulation of FAM135A Facilitates Perineural Invasion in Prostate Cancer. Arch Int J Cancer Allied Sci. 2022;2(2):67-79. https://doi.org/10.51847/bQH4fWO5RQ

cells contributes to tumor initiation, progression, and therapeutic resistance [5–7]. With the emergence of cancer neuroscience as a distinct research field, the influence of the neural microenvironment on tumor biology has gained substantial attention [5, 8, 9]. Perineural invasion (PNI), a pathological process characterized by tumor growth along or around nerves, is observed in 17–75% of PCa cases and is strongly associated with aggressive disease behavior and unfavorable clinical outcomes [10, 11]. Neurotransmitters [12, 13], neuropeptides [14, 15], and their corresponding receptors [16–18] not only serve as markers of disease progression and prognosis but also actively promote PCa advancement. Moreover, therapeutic strategies aimed at disrupting tumor–nerve interactions are increasingly recognized as promising approaches in oncology [19, 20]. Consequently, clarifying the molecular basis of PNI in PCa may uncover novel avenues for targeted intervention.

Gastrin-releasing peptide (GRP) is a neuropeptide originally characterized for its role in itch-specific signaling [21–23], and it has also been implicated in liver and kidney injury [24, 25], fear-associated learning processes [26], and pulmonary fibrosis [27]. Its receptor, gastrin-releasing peptide receptor (GRPR), is aberrantly overexpressed in multiple malignancies [28] and has been widely explored as a target for cancer imaging and radionuclide-based therapies [29, 30], particularly in prostate cancer [31, 32]. In addition, circulating pro–gastrin-releasing peptide has shown strong diagnostic utility in well-differentiated neuroendocrine tumors of the lung [33]. Although GRPR-targeted diagnostic and therapeutic strategies have progressed to clinical trials in PCa [31, 34, 35], the functional relevance of GRPR signaling in PCa-associated perineural invasion remains largely undefined.

In the present study, we performed a comparative transcriptomic analysis of prostate cancer specimens with and without PNI. Family with Sequence Similarity 135 Member A (FAM135A) is a highly conserved mammalian gene predominantly expressed in the brain, retina, and other normal tissues [36]. While alterations in FAM135A have been reported in pancreatic neuroendocrine tumors [37], its biological significance in PCa has not been previously clarified. Our analyses identified FAM135A as the most markedly upregulated gene in PNI-positive PCa samples. Subsequent experimental investigations demonstrated that suppression of FAM135A effectively limits tumor growth and neural invasion, supporting its role as a tumor-intrinsic driver. Notably, FAM135A exhibits predominant nuclear localization, and Teneurin Transmembrane Protein 3 (TENM3) was identified as a critical mediator of FAM135A-driven nerve invasion in PCa. Within this regulatory network, several neuroactive ligand–receptor pairs were altered, including GRPR, which was significantly upregulated in PNI-positive tumors. Finally, we demonstrated that GRPR signaling induces FAM135A expression through activation of the transcriptional regulator MED1. Collectively, this work provides the first evidence establishing FAM135A as a central regulator of perineural invasion in prostate cancer and proposes a novel therapeutic framework targeting tumor–nerve interactions.

Results and Discussion

Identification of FAM135A as a neural invasive marker in prostate cancer

Perineural invasion (PNI) is recognized as an independent indicator of poor prognosis and metastatic potential in prostate cancer [10], yet the molecular determinants driving this process remain insufficiently characterized. To comprehensively explore the genetic landscape associated with PNI, we reanalyzed transcriptomic data reported by Prueitt RL *et al*. [38], comparing PCa samples with documented PNI to those lacking this feature. This analysis revealed 124 transcripts, including both mRNAs and lncRNAs, that were differentially expressed between the two groups **(Figures 1a, 1b and Table 1)**. Of these, 77 genes were significantly upregulated in PNI-positive tumors—such as FAM135A, PSCA, CHRM2, and GABRA4—whereas 47 genes, including GUCY2D and NEUROD1, were downregulated. In addition to protein-coding genes, several lncRNAs showed notable alterations, with RP11-286E11.2 markedly increased and C1QTNF9B-AS1 significantly decreased in the PNI cohort.

Pathway enrichment analysis of these differentially expressed genes demonstrated significant overrepresentation of signaling pathways related to neuroactive ligand–receptor interaction, cell adhesion molecules, and the Notch signaling cascade **(Figure 1c)**, indicating their potential involvement in PNI development. Within the neuroactive ligand–receptor interaction pathway, ten genes exhibited significant differential expression **(Figure 1d)**. Six genes—Cholinergic Receptor Muscarinic 2 (CHRM2),

Cholinergic Receptor Muscarinic 4 (CHRM4), Gamma-Aminobutyric Acid Type A Receptor Subunit Alpha4 (GABRA4), 5-Hydroxytryptamine Receptor 2B (HTR2B), Vasoactive Intestinal Peptide Receptor 2 (VIPR2), and Gastrin-Releasing Peptide Receptor (GRPR)—were upregulated, whereas four genes—F2R Like Trypsin Receptor 1 (F2RL1), Relaxin 1 (RLN1), Relaxin 2 (RLN2), and Prostaglandin E Receptor 4 (PTGER4)—were downregulated. These observations align with previous reports implicating neuroactive ligand–receptor signaling in prostate cancer innervation and progression [16–18].

Among all 124 differentially expressed genes, FAM135A emerged as the most significantly elevated transcript in PNI-positive samples **(Figure 1e)**. To validate this association at the protein level, we examined pathologically confirmed PCa tissues with and without PNI using immunohistochemical analysis. FAM135A expression was markedly higher in PNI-positive tumors compared with non-PNI counterparts, supporting a strong positive association between FAM135A and perineural invasion **(Figure 1f)**. Quantitative assessment further demonstrated a significantly increased nuclear-to-cytoplasmic (N/C) ratio of FAM135A in PNI-positive specimens relative to non-PNI tumors **(Figure 1g)**, suggesting that nuclear enrichment of FAM135A may be functionally linked to neural invasive behavior in prostate cancer.

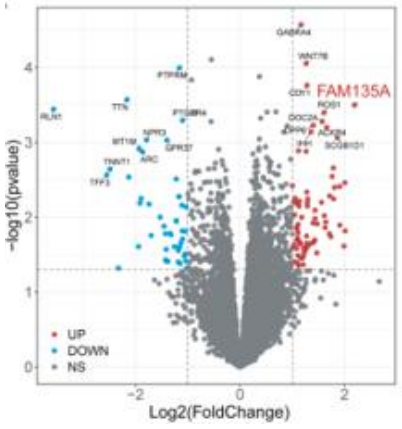

a)

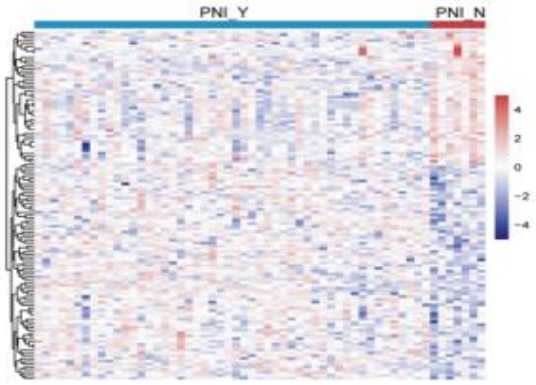

b)

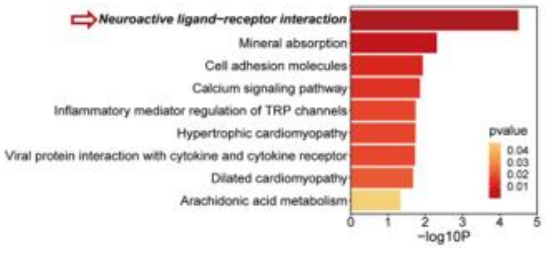

c)

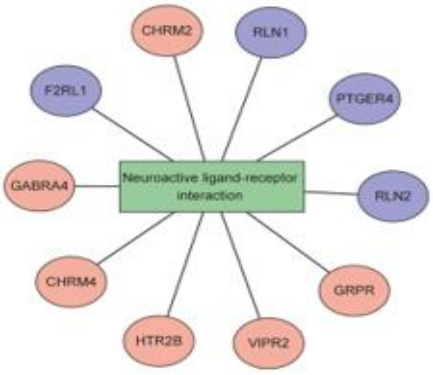

d)

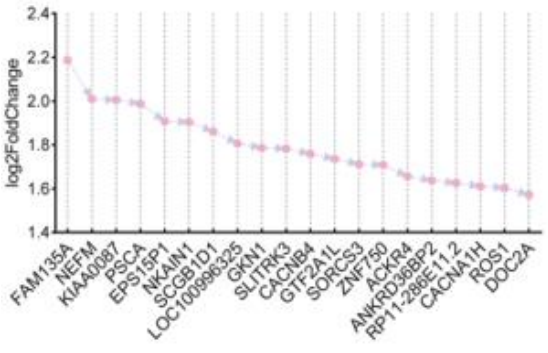

e)

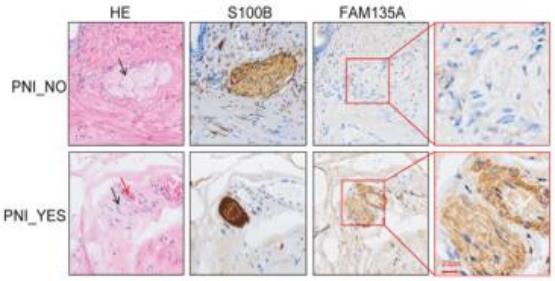

f)

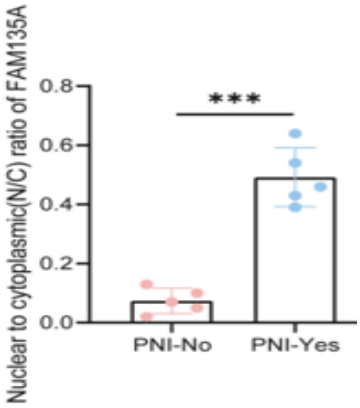

g)

Figure 1. Identification of FAM135A as a Key Indicator of Perineural Invasion in Prostate Cancer. (a) Genome-wide expression profiling comparing prostate cancer specimens with perineural invasion (PNI) to those lacking PNI, using the GSE10779 dataset; genes were considered significantly altered based on an FDR-corrected $P < 0.05$ and an absolute $\log_2$ fold change greater than 1. (b) Z-score–standardized heatmap illustrating the expression patterns of genes differentially expressed between PNI-positive and PNI-negative tumors. (c) Functional enrichment results highlighting the most overrepresented KEGG pathways among the differentially expressed genes identified in (A), generated using the DAVID platform; enrichment significance is displayed as $-\log_{10}$(P value). (d) List of the ten most strongly deregulated components of the KEGG "Neuroactive ligand–receptor interaction" pathway in the PNI comparison. (e) Ranking of the twenty genes showing the greatest expression increase in PNI-positive prostate cancer samples, ordered by $\log_2$ fold change magnitude. (f) Representative immunohistochemical visualization of FAM135A expression in histologically verified prostate cancer tissues with and without PNI; tumor cells are indicated by yellow arrows and neural structures by black arrows. Confirmation of PNI was achieved through dual staining for FAM135A and the Schwann cell marker S100 on adjacent serial sections, as detailed in the Methods. Scale bar = 20 µm. (g) Comparative quantification of the nuclear versus cytoplasmic distribution of FAM135A staining in PNI-negative and PNI-positive tumors, expressed as the nuclear-to-cytoplasmic (N/C) ratio. Values represent mean ± SD; $^{**}P < 0.01$ by Student's t test.

Table 1. Clinical characteristics of prostate cancer patients for immunohistochemical validation

No.	Group	Gleason Score	Tumor Area Ratio	Age	WHO /ISUP
P1	PNI	7	50%	71	3
P2	PNI	7	20%	70	2
P3	PNI	7	25%	71	2
P4	PNI	7	10%	71	2
P5	PNI	7	80%	69	3
P6	Non-PNI	7	15%	69	2
P7	Non-PNI	7	25%	66	2
P8	Non-PNI	7	2%	69	2
P9	Non-PNI	7	3%	68	2
P34	Non-PNI	7	20%	72	2

FAM135A drives neuroinvasive malignant traits in prostate cancer

To define the contribution of FAM135A to perineural invasion (PNI) in prostate cancer, we first evaluated its functional impact on prostate cancer cell behavior. Lentiviral short hairpin RNAs (shRNAs) specifically targeting FAM135A were generated and introduced into the androgen-independent DU145 and PC3 cell lines. Efficient suppression of FAM135A expression was stringently confirmed at both the transcript and protein levels by qRT-PCR and immunoblotting, respectively. Functional assays revealed that depletion of FAM135A markedly impaired tumor cell growth. Both DU145 and PC3 cells exhibited a pronounced reduction in proliferative capacity following FAM135A silencing, accompanied by a substantial decrease in clonogenic potential. In parallel, loss of FAM135A significantly enhanced tumor cell death rates, collectively indicating that FAM135A is required for maintaining prostate cancer cell survival and expansion.

Given that aggressive invasion and migration are prerequisites for neural infiltration, we next examined whether FAM135A influences these properties. Suppression of FAM135A led to a robust attenuation of invasive capacity **(Figures 2a and 2b)** as well as migratory activity **(Figures 2c and 2d)**, demonstrating that FAM135A supports the motile and invasive phenotype of prostate cancer cells.

To more directly model tumor–nerve interactions, we employed in vitro co-culture systems designed to recapitulate neural invasion. In a three-dimensional basement membrane matrix, PC3 or DU145 cells were co-cultured with PC12 neuronal cells, with tumor cells fluorescently labeled in red and PC12 cells in green **(Figure 2e)**. Quantitative assessment of tumor cell accumulation around PC12 neurites showed that FAM135A knockdown resulted in a marked reduction in the number and proportion of tumor cells encircling neuronal structures after 48 hours of co-culture **(Figures 2f and 2g)**. This finding indicates a genuine loss of neurotropic invasive capacity rather than a simple delay in migration.

To further validate these observations, a second co-culture model incorporating dorsal root ganglia (DRG) and prostate cancer cells embedded in a basement membrane matrix was established **(Figure 2h)**. Consistent with the PC12 model, FAM135A-deficient tumor cells demonstrated a significantly diminished ability to infiltrate and surround DRG structures **(Figures 2i and 2j)**.

Collectively, these in vitro data demonstrate that FAM135A is a critical regulator of malignant behaviors linked to neural invasion in prostate cancer. Importantly, interference with FAM135A not only suppresses tumor growth and motility but also disrupts tumor–nerve interactions, highlighting its potential as a therapeutic target for limiting perineural invasion.

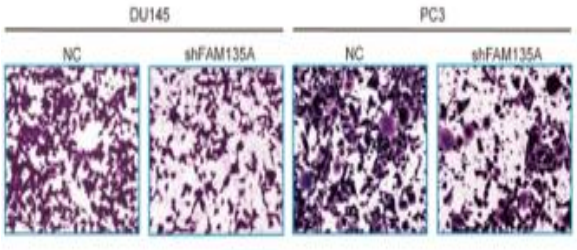

a)

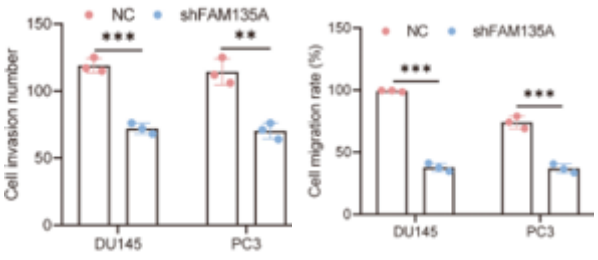

b)

d)

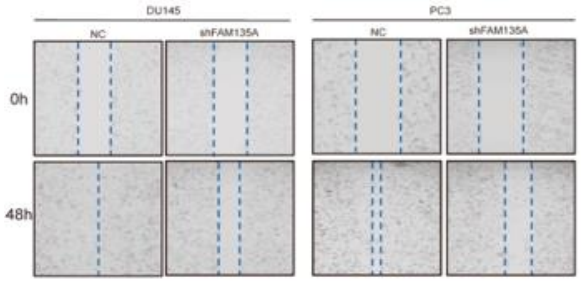

c)

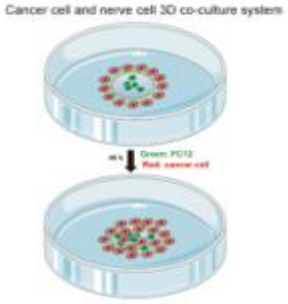

e)

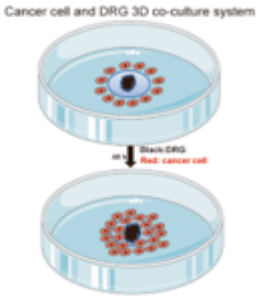

h)

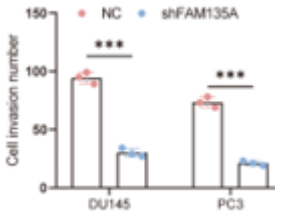

g)

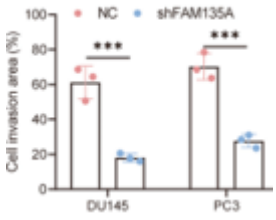

j)

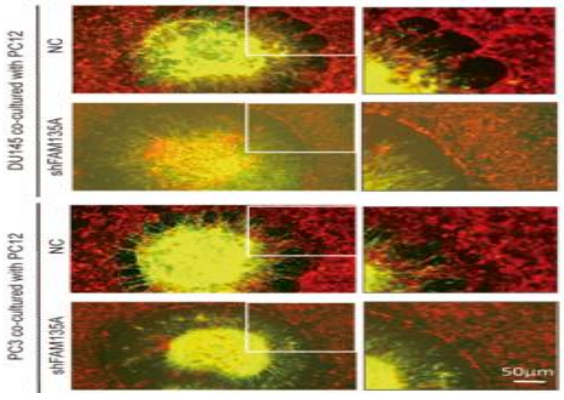

f)

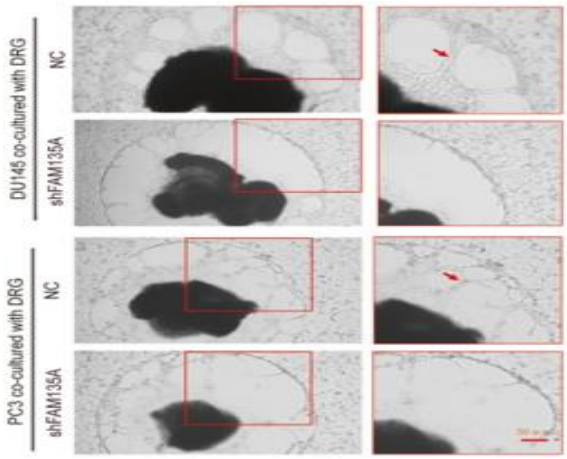

i)

Figure 2. Genetic suppression of FAM135A attenuates prostate cancer cell invasiveness and neurotropic potential.

(a–b) Transwell-based invasion assays demonstrating a marked reduction in invasive activity following FAM135A knockdown in prostate cancer cells.

(c–d) Scratch wound–healing assays showing a pronounced impairment in lateral cell migration upon FAM135A silencing.

(e) Diagrammatic representation of the three-dimensional Matrigel-based co-culture system used to model interactions between prostate cancer cells and neuronal cells.

(f–g) Fluorescence microscopy images illustrating decreased tumor cell encroachment toward neuronal processes after 48 hours of co-culture in the absence of FAM135A (scale bar: 50 µm).

(h) Schematic overview of the co-culture platform combining prostate cancer cells with dorsal root ganglion (DRG) neurons embedded in basement membrane matrix.

(i–j) Bright-field micrographs depicting reduced morphological engagement and infiltration of tumor cells into DRG structures following 48 hours of co-culture when FAM135A is suppressed (scale bar: 50 µm).

Statistical significance: **P < 0.01; ***P < 0.001.

To comprehensively assess the influence of FAM135A on tumor–nerve interactions in vivo, we established a sciatic nerve invasion mouse model by directly implanting prostate cancer cells with stable FAM135A knockdown or corresponding control cells into the sciatic nerve **(Figure 3a)**. Longitudinal evaluation revealed that tumors derived from FAM135A-deficient cells exhibited a substantially reduced volume within the sciatic nerve compared with controls **(Figure 3b)**, indicating impaired tumor propagation along neural structures.

Functional assessment further demonstrated that mice receiving control tumor cells developed significant deficits in hindlimb motor performance relative to non-tumor–bearing animals, whereas animals implanted with FAM135A-silenced cells retained significantly better motor function **(Figures 3c and 3d)**. These findings suggest that loss of FAM135A not only restricts tumor expansion but also alleviates tumor-induced neural dysfunction.

Histopathological examination using hematoxylin and eosin staining, together with Ki67 immunostaining, revealed a marked reduction in perineural invasion and proliferative activity in tumors lacking FAM135A **(Figure 3e)**. To ensure that these phenotypic differences were attributable to durable gene suppression, immunohistochemical analysis of harvested sciatic nerve tumors was performed at the study endpoint. Consistent with in vitro validation, FAM135A expression remained significantly diminished in the shFAM135A group compared with controls **(Figures 3f and 3g)**, confirming stable gene silencing throughout the experimental period.

Taken together, these integrated in vitro and in vivo findings establish FAM135A as a critical mediator of aggressive prostate cancer behavior. Its inhibition not only curtails tumor growth and invasiveness but also disrupts tumor–nerve crosstalk and preserves neural function, supporting FAM135A as a promising therapeutic target for limiting prostate cancer progression and perineural invasion.

a)

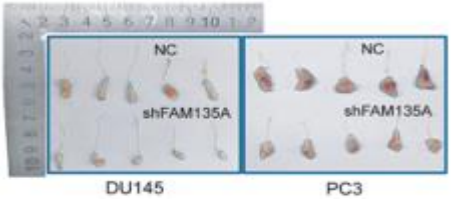

b)

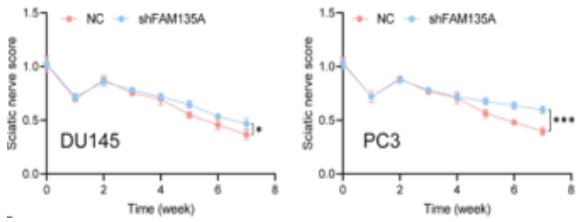

c)

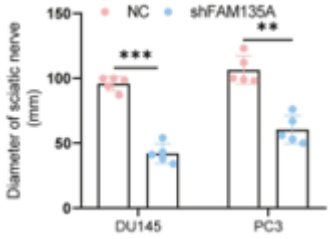

d)

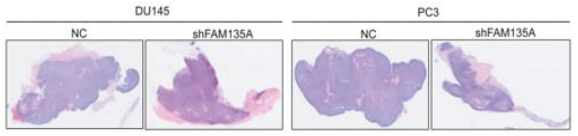

e)

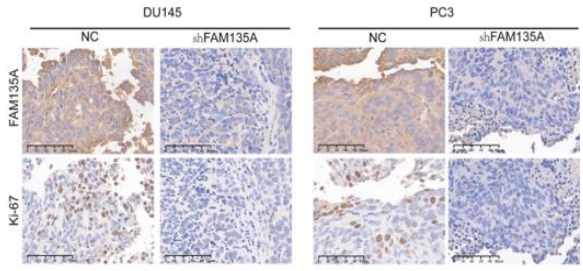

f)

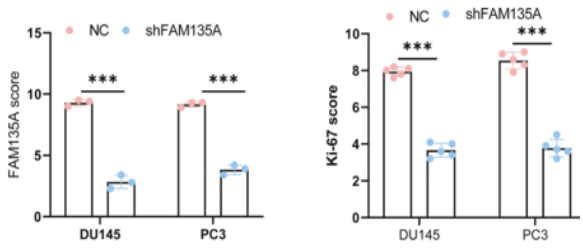

g

Figure 3. Sciatic Nerve Mouse Model Demonstrates That FAM135A Silencing Suppresses Tumor Growth and Preserves Neuromuscular Function

(a) Implantation of prostate cancer cells into the mouse sciatic nerve induces observable motor deficits.

(b) Dissection of sciatic nerve tumors shows that FAM135A knockdown reduces both tumor volume and longitudinal spread along the nerve.

(c) Motor function scoring reveals significant improvement in mice receiving FAM135A-silenced cells.

(d) Compared with controls, the sciatic nerve diameter is notably smaller in the FAM135A-deficient group.

(e) Hematoxylin and eosin staining highlights histological alterations in tumor tissues within the nerve.

(f–g) Ki67 immunostaining indicates a marked reduction in proliferative activity in tumors with FAM135A silencing. Statistical significance: *P < 0.05; **P < 0.01; ***P < 0.001.

RAN regulates nuclear import of FAM135A

To explore the mechanistic role of FAM135A in prostate cancer cells, we first assessed its subcellular localization. Analysis using the THPA database and immunofluorescence revealed nuclear enrichment of FAM135A, and further imaging in PC3 and DU145 cells showed that FAM135A resides in both the cytoplasm and nucleus **(Figure 4a)**, suggesting a potential transcriptional regulatory function.

To identify factors controlling nuclear translocation of FAM135A, we focused on nucleocytoplasmic transport, a process implicated in tumor progression [39]. Co-immunoprecipitation (Co-IP) followed by mass spectrometry identified multiple FAM135A-interacting proteins, including three nucleocytoplasmic transport–related candidates: SRRM1, RNPS1, and **RAN (Figure 4b)**. Because RAN is known to facilitate tumor progression through abnormal nuclear transport [40], we investigated its role in FAM135A localization. Co-IP and Western blot confirmed direct binding between RAN and FAM135A **(Figure 4c)**.

Next, RAN was silenced in PC3 and DU145 cells **(Figure 4d)**, and nuclear-cytoplasmic fractionation was performed to quantify FAM135A distribution. RAN knockdown significantly decreased nuclear FAM135A levels (nFAM135A), while cytoplasmic FAM135A (cFAM135A) remained largely unchanged **(Figure 4e)**, with GAPDH and PCNA used as cytoplasmic and nuclear controls, respectively. In contrast, individual knockdown of SRRM1 or RNPS1 had no appreciable effect on nuclear FAM135A abundance.

Finally, immunofluorescence confirmed co-localization of FAM135A with RAN in the nucleus **(Figure 4g)**, indicating that among its interacting partners, RAN is the

primary mediator responsible for FAM135A nuclear translocation.

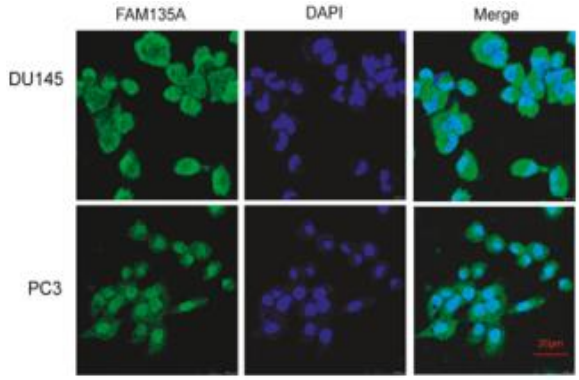

a)

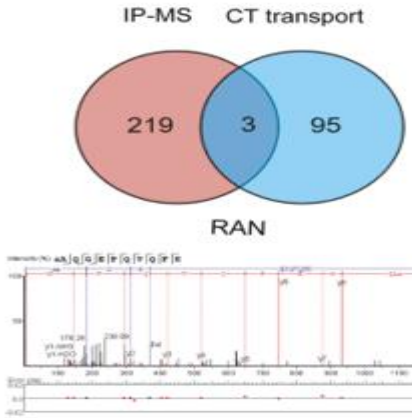

b)

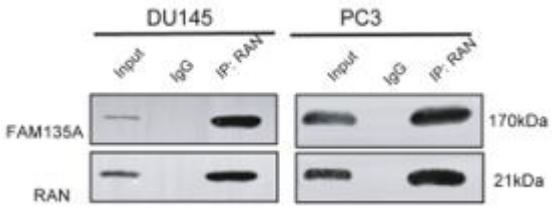

c)

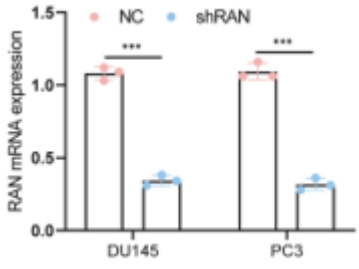

d)

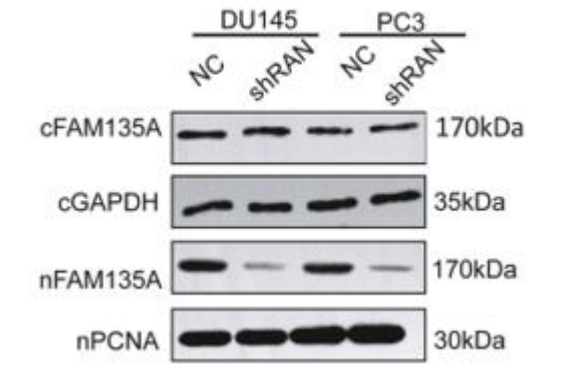

e)

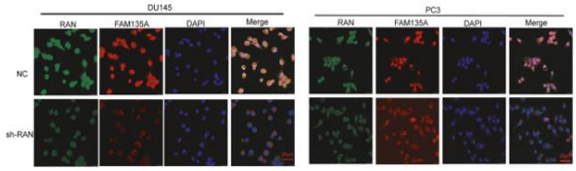

f)

Figure 4. RAN facilitates the nuclear import of FAM135A

(a) Immunofluorescence staining demonstrates predominant nuclear localization of FAM135A in prostate cancer cells (scale bar: 20 μm).

(b) FAM135A was tagged with a Flag epitope, and co-immunoprecipitation coupled with mass spectrometry was used to identify interacting proteins, highlighting three candidates involved in nucleocytoplasmic transport: SRRM1, RNPS1, and RAN.

(c) Co-immunoprecipitation of RAN confirmed its direct interaction with FAM135A, validated by Western blot analysis.

(d) Silencing efficiency of RAN was verified in PCa cells.

(e) Nuclear-cytoplasmic fractionation following RAN knockdown revealed a marked reduction of nuclear FAM135A, whereas cytoplasmic levels remained largely unchanged.

(f) Immunofluorescence in DU145 and PC3 cells confirmed co-localization of RAN and FAM135A within the nucleus (scale bar: 20 μm). Statistical significance: ***P < 0.001.

Integrated RNA-Seq and ChIP-Seq analyses identify TENM3 as a novel transcriptional target of FAM135A

To investigate the downstream regulatory network of FAM135A in prostate cancer, RNA sequencing was performed on PC3 and DU145 cells following FAM135A knockdown, compared with control cells.

Analysis revealed 1,026 and 212 significantly differentially expressed genes (DEGs) in PC3 **(Figure 5a)** and DU145 cells **(Figure 5b)**, respectively.

A combined analysis of DEGs common to both cell lines identified 27 genes consistently altered upon FAM135A silencing **(Figure 5c)**. Among these, 23 genes were upregulated (e.g., ABCA1) and 4 genes were downregulated, including TENM3, suggesting that TENM3 may act as a direct transcriptional target of FAM135A and mediate its effects in prostate cancer cells.

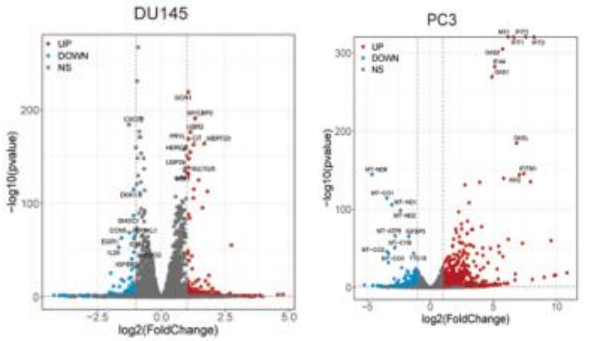

a) b)

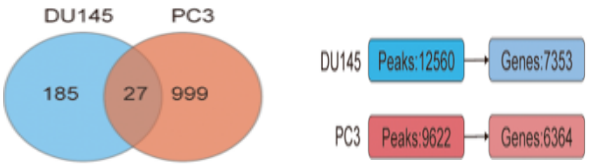

c)

e)

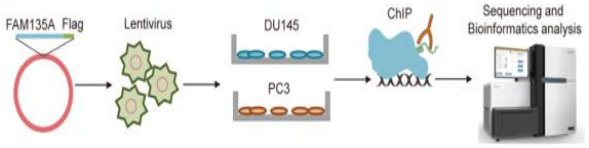

d)

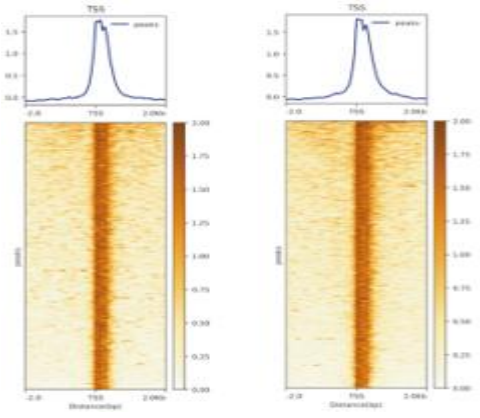

g)

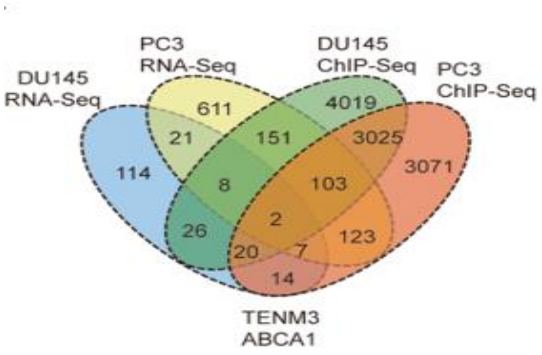

f)

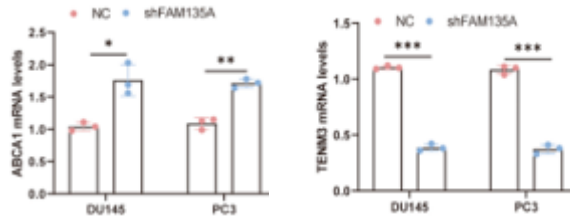

h) i)

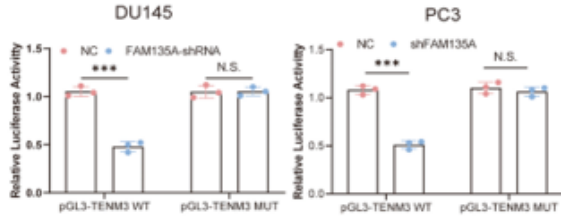

j)

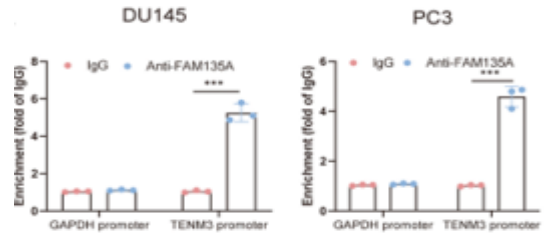

k)

Figure 5. RNA-Seq and ChIP-Seq Reveal Novel Transcriptional Targets of FAM135A. (a–b) Transcriptomic profiling of genes significantly altered upon FAM135A knockdown in DU145 and PC3 cells, using an FDR-adjusted p-value < 0.05 and |log2 fold change| >1; (c) Integration of differential gene sets from both cell lines identified 27 shared differentially expressed genes; (d) Construction of a Flag-tagged FAM135A system and identification of putative target genes via ChIP-Seq; (e) ChIP-Seq revealed FAM135A binding peaks in DU145 and PC3 cells, with corresponding genes annotated; (f) Combined RNA-Seq and ChIP-Seq analysis identified two overlapping genes, TENM3 and

ABCA1; (g) Heatmap depicting the localization of FAM135A binding peaks around gene transcription start sites (TSS); (h) FAM135A silencing markedly reduced ABCA1 mRNA levels; (i) FAM135A silencing significantly decreased TENM3 mRNA levels; (j) Dual-luciferase reporter assay demonstrated that promoter sequence mutation abolished FAM135A binding to the TENM3 promoter; (k) ChIP-PCR confirmed FAM135A binding to the TENM3 promoter *** $P < 0.001$.

To elucidate the transcriptional regulatory role of FAM135A in prostate cancer perineural invasion (PNI), we generated a Flag-tagged FAM135A construct and conducted chromatin immunoprecipitation sequencing (ChIP-Seq) to identify its target genes **(Figure 5d)**. Peak calling in PC3 and DU145 cells followed by gene annotation revealed 12,560 peaks in DU145, corresponding to 7,353 genes, and 9,622 peaks in PC3, corresponding to 6,364 genes **(Figure 5e)**. Notably, 13.94% of peaks in DU145 and 13.5% in PC3 were located in promoter regions, exemplified by the ID2 gene **(Figure 5f)**. Integrating RNA-Seq and ChIP-Seq results indicated that, among the 27 commonly dysregulated genes, two—TENM3 and ABCA1—also displayed FAM135A binding in ChIP-Seq **(Figure 5f)**. The distribution of FAM135A binding peaks near TSS loci is depicted in a heatmap **(Figure 5g)**.

Subsequently, FAM135A was silenced, and expression of ABCA1 and TENM3 was assessed by quantitative real-time PCR (qRT-PCR). FAM135A knockdown significantly upregulated ABCA1 **(Figure 5h)** while downregulating TENM3 mRNA **(Figure 5i)**, indicating that FAM135A promotes TENM3 expression. Given that ABCA1 functions as a well-established tumor suppressor in prostate cancer by modulating cholesterol metabolism, its increased expression upon FAM135A silencing [41, 42] led us to prioritize TENM3 for further study. TENM3 has documented roles in neuronal development and neuroblastoma tumorigenesis [43], suggesting it may serve as a FAM135A-induced target in prostate cancer PNI. To validate FAM135A's transcriptional activation of TENM3, dual-luciferase reporter assays confirmed its effect on TENM3 promoter activity **(Figure 5j)**, and ChIP-PCR further verified significant enrichment of FAM135A at the TENM3 promoter **(Figure 5k)**. Collectively, these data demonstrate that FAM135A activates TENM3 transcription to enhance its expression.

FAM135A Promotes Perineural Invasion in Prostate Cancer via TENM3 Activation. To investigate TENM3's role in FAM135A-mediated PNI, immunohistochemical (IHC) staining was performed on PNI and non-PNI prostate cancer tissues, revealing elevated TENM3 expression in PNI samples **(Figures 6a and 6b)**. The efficiency of TENM3 knockdown was confirmed by qRT-PCR and Western blot, showing a marked reduction of TENM3 levels. Functional assays demonstrated that TENM3 silencing significantly decreased tumor cell invasion into nerves in transwell co-culture **(Figures 6c and 6d)** and DRG-PCa co-culture models **(Figures 6e and 6f)**. In vivo, TENM3 knockdown reduced sciatic nerve tumor volume **(Figure 6g)** and improved mouse sciatic nerve functional scores **(Figure 6h)**, indicating amelioration of nerve impairment. H&E staining **(Figure 6i)** and Ki67 IHC **(Figure 6j and 6k)** revealed that TENM3 depletion also lowered Ki67 proliferation indices. These findings collectively indicate that TENM3 knockdown substantially suppresses prostate cancer PNI progression.

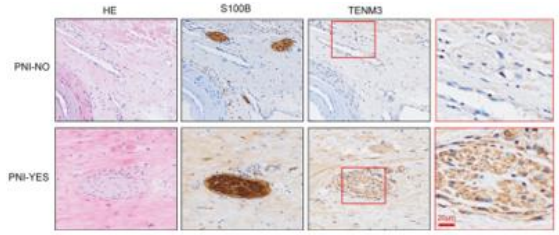

a)

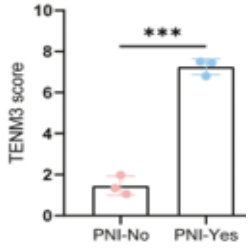

b)

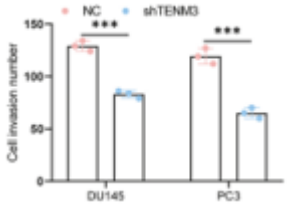

d)

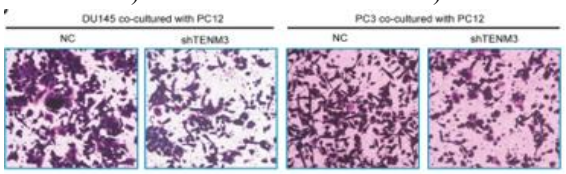

c)

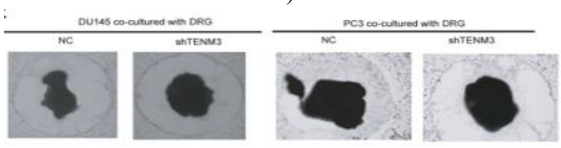

e)

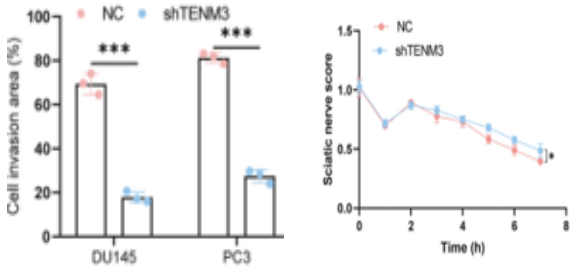

f) h)

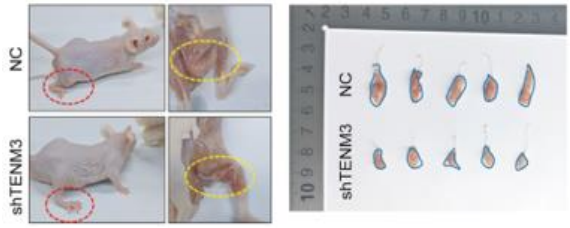

g)

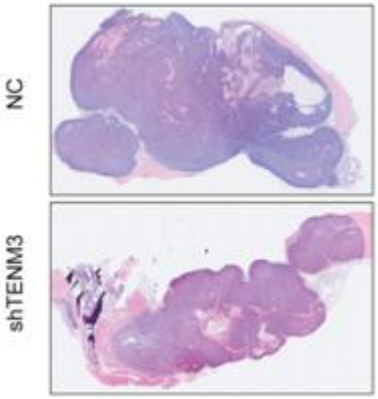

i)

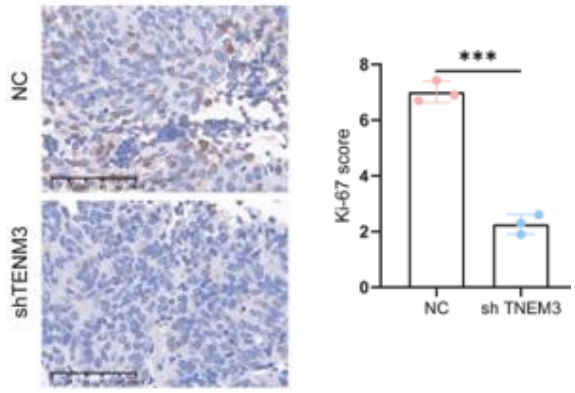

j) k)

Figure 6. TENM3 is highly upregulated in PNI-positive prostate cancer and facilitates neural invasion. (a-b) Immunohistochemical analysis demonstrates marked TENM3 overexpression in prostate cancer tissues exhibiting perineural invasion (scale bar: 20 μm). (c-d) Transwell co-culture assays with PC3 neuronal cells reveal that TENM3 knockdown significantly reduces the ability of tumor cells to invade toward neurons. (e-f) In the DRG-tumor cell co-culture system, silencing TENM3 markedly diminishes tumor cell infiltration toward DRG neurons after 48 hours. (g-h) In vivo, injecting TENM3-deficient tumor cells into the mouse sciatic nerve leads to smaller tumors and improved neurological outcomes. (i) H&E staining of tumors derived from control and FAM135A-silenced cells; (j-k) IHC analysis shows that FAM135A knockdown substantially lowers Ki67 expression (scale bar: 60 μm), *P < 0.05; ***P < 0.001.

To further elucidate TENM3's involvement in FAM135A-driven perineural invasion, we overexpressed TENM3 in DU145 and PC3 cells with stable FAM135A knockdown, confirming successful TENM3 upregulation in this context. In both Transwell co-culture **(Figures 7a and 7b)** and DRG-tumor cell co-culture assays **(Figures 7c and 7d)**, TENM3 overexpression partially rescued the decrease in tumor cell invasion into nerves caused by FAM135A depletion. Similarly, in the DU145 sciatic nerve implantation model **(Figure 7e)**, TENM3 upregulation partially counteracted the tumor growth suppression induced by FAM135A silencing **(Figure 7f)** and improved functional scores of the affected sciatic nerve **(Figure 7g)**. Histopathological evaluation **(Figure 7h)** and Ki67 IHC staining **(Figures 7i and 7j)** further confirmed that TENM3 restoration mitigates the inhibitory effects of FAM135A knockdown. Collectively, these findings indicate that TENM3 is a crucial mediator of FAM135A-driven perineural invasion in prostate cancer.

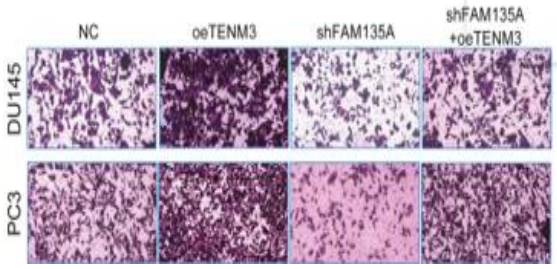

a)

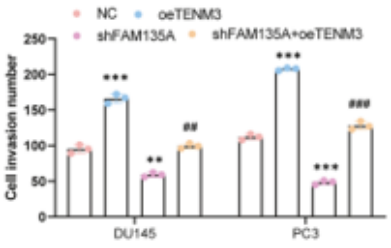

b)

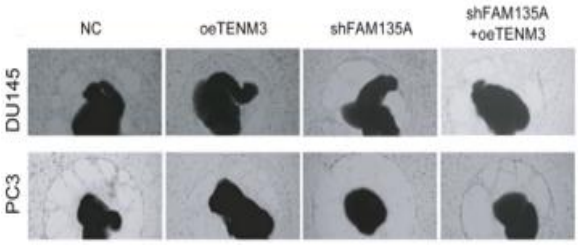

c)

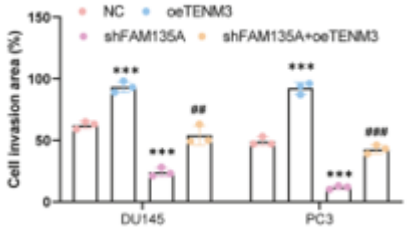

d)

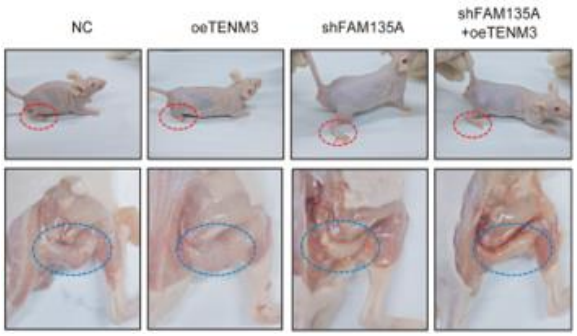

e)

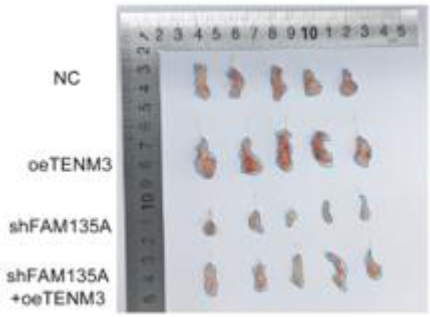

f)

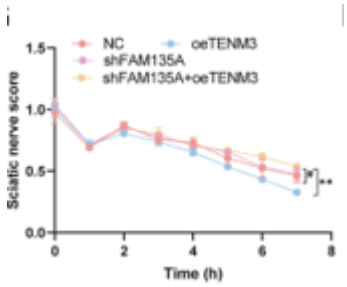

g)

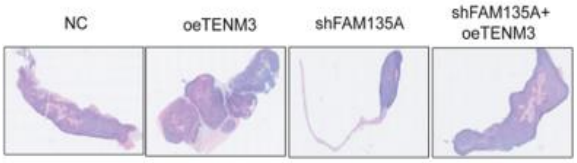

h)

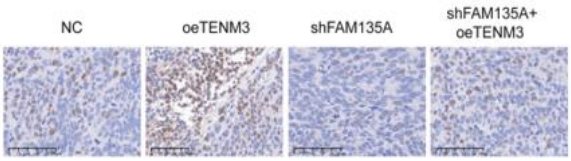

i)

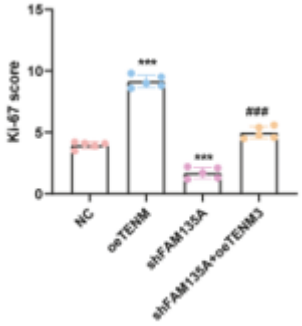

j)

Figure 7. FAM135A facilitates neural invasion of cancer via TENM3. (a-b) Transwell co-culture assays with PC3 neuronal cells demonstrated that overexpressing TENM3 in tumor cells with silenced FAM135A restores their capacity to invade neurons, counteracting the inhibitory effect of FAM135A; (c-d) Using the tumor cell–DRG co-culture system, TENM3 overexpression similarly rescues the impaired invasion of FAM135A-silenced tumor cells towards DRG; (e-f) In vivo, injecting tumor cells with TENM3 overexpression and FAM135A knockdown into the mouse sciatic nerve revealed that TENM3 reverses the suppressive effects of FAM135A on tumor progression and neurological function recovery; (g) Sciatic nerve motor function scores for groups with TENM3 overexpression,

FAM135A silencing, or combined treatment; (h) H&E staining of tumor tissues from the same experimental groups; (i-j) Ki67 immunostaining of tumor samples across these groups (scale bar: 60 μm); * indicates comparison with NC group (*P < 0.05; **P < 0.01; ***P < 0.001), # indicates comparison with shFAM135A group (#P < 0.05; ##P < 0.01; ###P < 0.001).

FAM135A expression is induced by Gastrin-Releasing Peptide Receptor (GRPR). Given that FAM135A is markedly upregulated in PNI samples and that PNI is likely driven by Neuroactive ligand–receptor interactions, we sought to identify which ligand–receptor pair might trigger FAM135A overexpression in PNI. Analysis of ten neuroactive ligands and receptors revealed that only GRPR exhibited a strong positive correlation with FAM135A (Pearson r = 0.3788, p < 0.001) **(Figure 8a)**, suggesting GRPR as a potential inducer. Previous studies indicate that GRPR is frequently overexpressed in human prostate cancer, and radiolabeled GRPR ligands have shown utility for PET imaging of prostate tumors [31, 34, 44].

To determine whether GRPR regulates FAM135A, we first silenced GRPR and observed a significant reduction in FAM135A expression **(Figure 8b)**. Treatment of prostate cancer cell lines with the non-peptide GRPR antagonist PD176252 [28] similarly decreased FAM135A levels, mirroring the effect of RNA interference **(Figure 8c)**. Conversely, administration of human recombinant GRP (hrGRP) led to a dose-dependent increase in FAM135A expression **(Figure 8d)**.

Mechanistically, previous reports indicate that GRPR activates ERK phosphorylation [45], which in turn drives MED1 phosphorylation and transcriptional activation [46]. Consistent with this, Western blot analysis showed that GRPR knockdown in DU145 and PC3 cells significantly reduced phosphorylated ERK (p-ERK) and phosphorylated MED1 (p-MED1) levels **(Figures 8e and 8f)**. Further investigation into transcriptional regulation of FAM135A revealed a strong MED1 binding peak within its promoter region **(Figure 8g)**. Luciferase reporter assays confirmed that MED1 directly targets the FAM135A promoter, and MED1 silencing suppressed FAM135A transcriptional activity **(Figures 8h and 8i)**. Collectively, these findings indicate that GRPR regulates FAM135A expression through MED1-mediated transcription within the p-ERK/p-MED1 signaling axis.

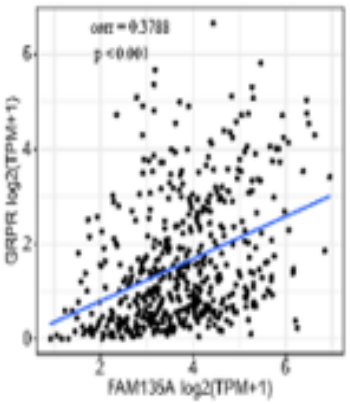

a)

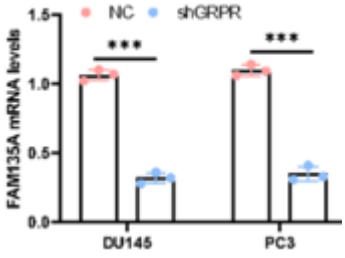

b)

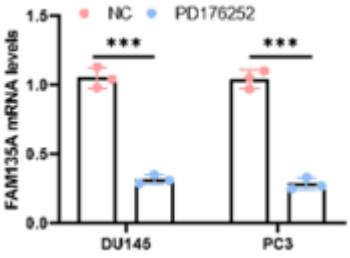

c)

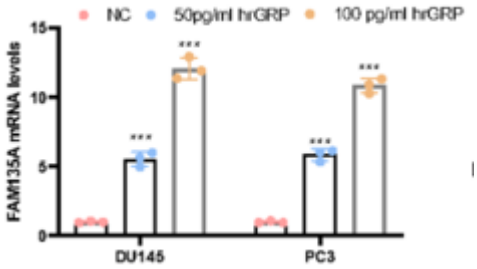

d)

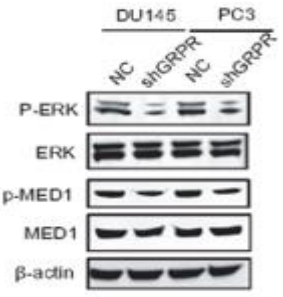

e)

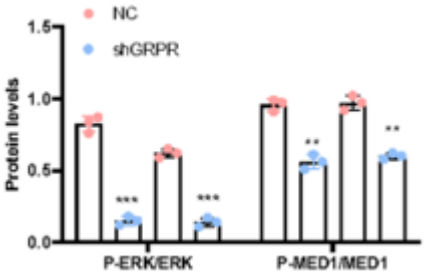

f)

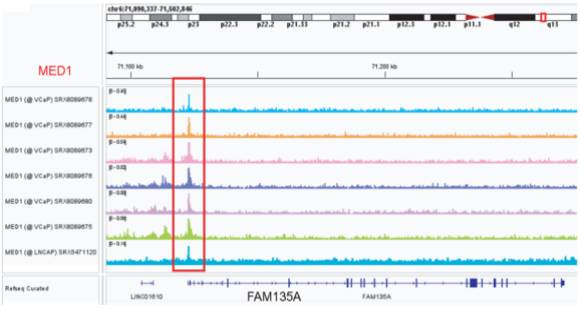

g)

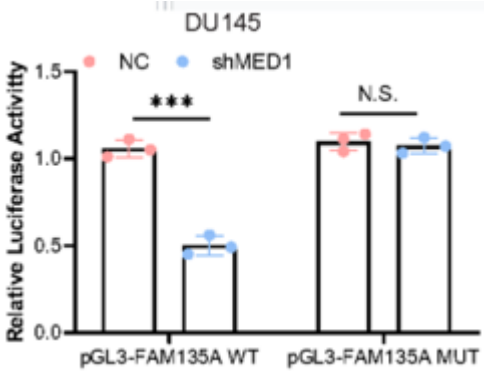

h)

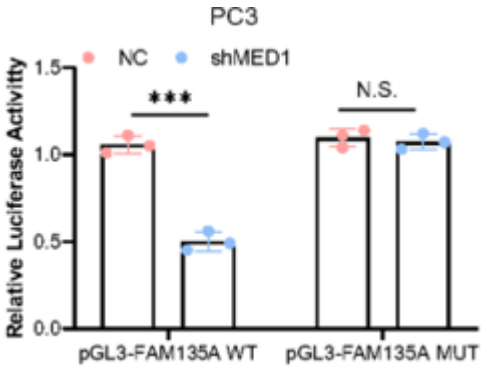

i)

Figure 8. FAM135A transcriptionally drives TENM3 expression. (a) Correlation analysis reveals a significant positive relationship between GRPR and FAM135A (Pearson r = 0.3788, $p < 0.001$); (b) GRPR knockdown results in decreased FAM135A expression; (c) Treatment with a GRPR inhibitor markedly lowers FAM135A levels; (d) FAM135A expression rises proportionally with increasing doses of hrGRP; (e-f) GRPR silencing reduces phosphorylated ERK (p-ERK) and phosphorylated MED1 (p-MED1) levels; (g) MED1 exhibits binding peaks upstream of the FAM135A promoter; (h-i) Luciferase reporter assays confirm that MED1 activates FAM135A transcription (**P < 0.01; ***P < 0.001).

Functional conservation of the GRPR–FAM135A–TENM3 axis in AR-positive prostate cancer cells. Considering the pivotal role of the androgen receptor (AR) in most prostate cancers and its reported involvement in PNI, we investigated whether the GRPR–FAM135A–TENM3 signaling cascade operates in AR-positive cells. Using the LNCaP cell line, we first confirmed that GRPR regulation of FAM135A is preserved: both GRPR shRNA and the antagonist PD176252 significantly suppressed FAM135A expression, whereas the agonist hrGRP enhanced it **(Figures 9a and 9c)**. Next, efficient knockdown of FAM135A was achieved in LNCaP cells **(Figure 9d)**. Consistent with observations in AR-negative cells, FAM135A silencing in LNCaP significantly impaired tumor cell invasion in Transwell assays **(Figures 9e and 9f)**, reduced invasive behavior in the LNCaP–PC12 co-culture system **(Figures 9g and 9h)**, and markedly decreased invasion toward DRG neurons in the co-culture model **(Figures 9i and 9j)**. Additionally, qRT-PCR analysis demonstrated that TENM3 mRNA levels

declined upon FAM135A knockdown **(Figure 9k)**, indicating that nuclear FAM135A continues to transcriptionally regulate TENM3 in an AR-positive context. Together, these results suggest that the GRPR–FAM135A–TENM3 axis operates alongside canonical AR signaling in the tested models.

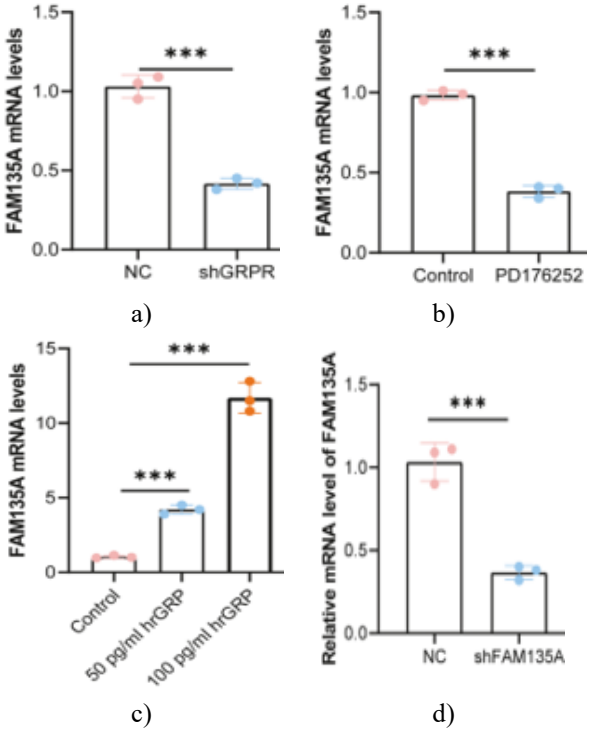

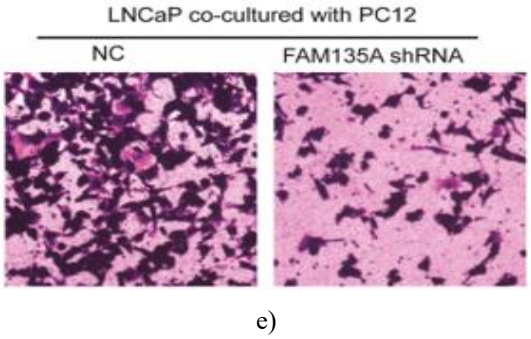

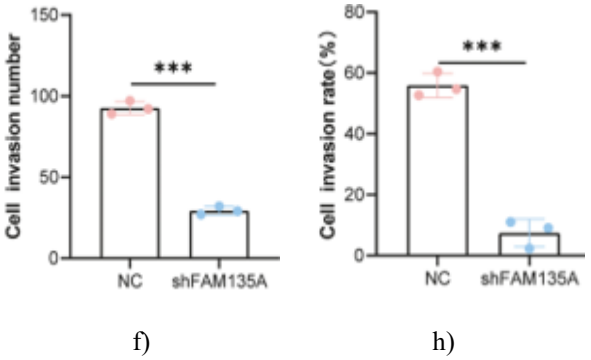

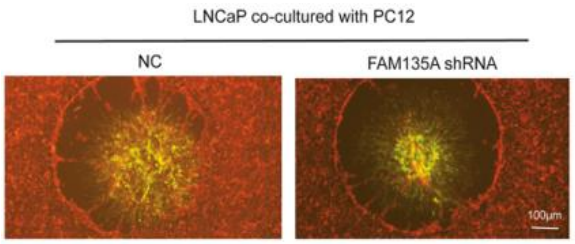

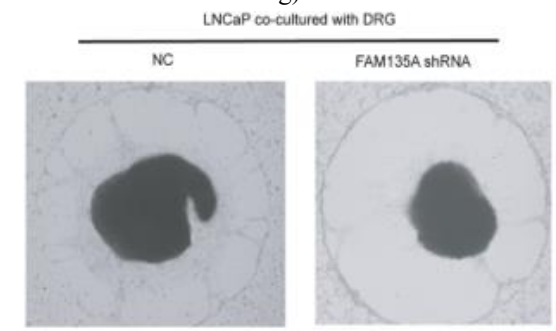

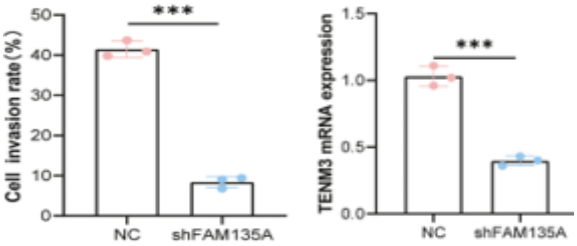

Figure 9. The GRPR–FAM135A–TENM3 axis is functionally active in AR-positive prostate cancer cells. (a) FAM135A mRNA levels in LNCaP cells after treatment with the GRPR antagonist PD176252. (b) FAM135A expression following GRPR knockdown in LNCaP cells. (c) Dose-dependent increase of FAM135A mRNA in response to the GRPR agonist human recombinant GRP (hrGRP). (d) Validation of FAM135A knockdown efficiency by qRT-PCR in LNCaP cells. (e-f) Transwell invasion assays showing that silencing FAM135A markedly reduces the invasive capacity of LNCaP cells, with quantitative data (e) and representative images (f). (g-h) Tumor cell–PC12 neuron co-culture assays demonstrating that FAM135A knockdown impairs LNCaP cell invasion toward neurons; quantitative analysis (g) and representative fluorescence images (h) are shown (scale bar: 100 μm; red: tumor cells; green: PC12 neurons). (i-j) Tumor cell–DRG co-culture experiments confirming reduced neural invasion upon FAM135A silencing, with quantitative

(i) and representative bright-field images (j). (k) qRT-PCR showing downregulation of TENM3 mRNA after FAM135A knockdown. Data are presented as mean ± SD; *p < 0.05, **p < 0.01, ***p < 0.001.

Perineural invasion (PNI) represents a frequent pathological feature and adverse prognostic factor in prostate cancer, yet its underlying molecular mechanisms remain incompletely defined [10, 47]. Neuropeptides, neurotransmitters, and their corresponding receptors likely facilitate PNI by enhancing the chemotactic behavior of tumor cells toward nerves [12, 13, 15, 48]. This study aimed to dissect the mechanisms of PNI, focusing on how FAM135A drives tumor invasion of nerves and revealing novel neuropeptide-regulated, tumor-intrinsic pathways via GRPR.

Our analysis identified differential expression of neuro-ligand receptors in PNI-positive prostate cancer samples. Notably, GRPR and VIPR2 were elevated in PNI, alongside acetylcholine receptors CHRM2 and CHRM4, GABA receptor GABRA4, and serotonin receptor HTR2B, whereas RLN1 and RLN2 were significantly downregulated. These findings suggest that PNI may arise through cooperative signaling by neurotransmitters and neuropeptides, consistent with prior studies highlighting their roles in tumor–nerve interactions [12–15]. While GRPR has been implicated in prostate cancer, the precise downstream effectors were previously unclear.

FAM135A is highly conserved across species. In our study, silencing FAM135A not only suppressed malignant phenotypes, including proliferation and invasion, but also significantly impaired tumor nerve invasion. These effects were validated in vitro using tumor cell–neuron and tumor cell–DRG co-culture assays with Matrigel, and in vivo using a mouse sciatic nerve tumor model that recapitulates neuro-oncological interactions. These findings highlight FAM135A as a potential therapeutic target for mitigating PNI and disease progression in prostate cancer.

FAM135A localizes predominantly to the nucleus, prompting us to investigate its nuclear translocation. We identified RAN (RAS-related nuclear protein), a small GTP-binding protein critical for nuclear transport of RNA and proteins, as essential for FAM135A nuclear import. RAN has previously been described as an AR co-activator [49], and inhibition of RAN markedly reduced nuclear localization of FAM135A, indicating its necessity for FAM135A nuclear transport and suggesting RAN's involvement in prostate cancer nerve invasion independent of AR signaling.

Recognizing that FAM135A enters the nucleus, we explored its role as a transcriptional regulator. ChIP-Seq after FAM135A silencing revealed global transcriptional remodeling in prostate cancer cells. Integration with RNA-Seq data identified TENM3 and ABCA1 as FAM135A-regulated targets. ABCA1, a tumor suppressor that inhibits progression via cholesterol metabolism, was upregulated following FAM135A knockdown [41, 42]. Given ABCA1's established role, we focused on TENM3, previously known for neural circuit assembly [50, 51] and implicated in cancer through TENM3–ALK fusions in neuroblastoma [43] and poor prognosis in esophageal cancer [52]. Our experiments demonstrated that TENM3 functions similarly to FAM135A in promoting PNI in prostate cancer cells.

Collectively, these findings define a FAM135A–TENM3 axis that drives tumor neural invasion, establishing a novel molecular link underlying PNI pathogenesis in prostate cancer.

An intriguing insight from our integrated omics analysis is that, although FAM135A occupies promoter regions of roughly 7,000–8,000 genes, only a very small fraction (~0.2%, including TENM3 and ABCA1) displayed consistent transcriptional alterations upon FAM135A knockdown. This pattern is common in studies of transcriptional regulation and can be explained by several biological mechanisms. First, not all transcription factor–DNA interactions lead to functional changes; some may represent "poised" or "pioneer" binding events that require additional cofactors or specific cellular contexts to modulate gene expression [53]. Second, FAM135A binding may contribute to structural or chromatin-organizing roles without directly influencing transcription rates of nearby genes. Third, cellular compensatory networks and transcriptional redundancies can buffer the loss of a single regulator, with only the most sensitive nodes exhibiting significant expression changes [54]. The identification and validation of TENM3 from this small, high-confidence subset highlights its critical function as a downstream effector of nuclear FAM135A in promoting PNI.

Within the neural ligand-enriched microenvironment of prostate cancer, we identified GRPR as a major inducer of FAM135A transcription, which can be upregulated by GRP or suppressed using GRPR antagonists. This finding

offers a potential therapeutic avenue for targeting PNI and tumor–nerve interactions, including possible clinical applications of GRPR inhibitors. Mechanistically, GRPR's induction of FAM135A appears to be mediated by the transcription factor MED1, which directly activates FAM135A transcription. Moreover, given that p-ERK is involved in regulating the GRPR–MED1–FAM135A axis, inhibitors of p-ERK may also offer a strategy to impede PNI in prostate cancer, and these approaches will be investigated in future studies.

Although our experiments demonstrate that prostate cancer cells respond to exogenous GRP, the in vivo source of GRP within the prostate tumor microenvironment remains to be elucidated. Potential contributors include: (1) neuroendocrine cells, which are especially prominent in advanced or therapy-resistant prostate cancer; (2) autocrine or paracrine secretion from subsets of tumor cells themselves, as seen for other neuropeptides in cancer; or (3) innervating neurons or stromal cells within the tumor microenvironment, consistent with concepts in cancer neuroscience. Spatially resolved techniques will be essential to precisely map GRP sources in PNI-positive prostate tumors.

To extend the clinical relevance beyond AR-independent models, we confirmed the functionality of the GRPR–FAM135A–TENM3 axis in AR-positive LNCaP cells. The conserved operation of this pathway in both AR-negative and AR-positive contexts suggests that it may represent a common mechanism driving PNI, potentially acting in parallel with or independently of canonical AR signaling, thereby broadening the patient population who could benefit from targeted therapies against this axis.

A key limitation of our study is that functional experiments employed shRNA-mediated knockdown, which depletes both cytoplasmic and nuclear FAM135A. Therefore, the distinct contributions of nuclear FAM135A (nFAM135A) versus cytoplasmic FAM135A (cFAM135A) to malignant phenotypes remain to be defined. Our data show that FAM135A nuclear translocation is actively mediated by RAN, and immunohistochemical analysis revealed a significantly higher nuclear-to-cytoplasmic FAM135A ratio in PNI-positive tumors, strongly implicating nFAM135A as functionally important. Future studies employing engineered FAM135A variants restricted to the nucleus (via nuclear localization signals) or retained in the cytoplasm (via nuclear export signals) will enable precise dissection of nFAM135A's transcriptional regulatory functions from potential cytoplasmic roles. In parallel, deeper exploration of signaling pathways and post-translational modifications governing FAM135A subcellular localization represents a valuable direction for follow-up research.

The relationship between PNI and metastasis also warrants consideration. PNI can facilitate tumor dissemination independently of lymphatic or vascular routes. Our in vivo model focused on local tumor burden along the sciatic nerve and its impact on motor function, without systematically assessing distant metastases in organs such as the lungs or liver. This represents a limitation. The possibility that the GRPR–FAM135A–TENM3 axis could also prime tumor cells for distant neural-mediated spread is compelling and warrants dedicated studies involving longer follow-up and sensitive detection of disseminated tumor cells in remote organs or neural ganglia.

Beyond mechanistic insights, these findings have translational potential. The pronounced overexpression of FAM135A in PNI-positive tumors and its central role in promoting neuro-invasive phenotypes nominate it as a promising biomarker for identifying patients at higher risk for nerve-centric disease progression, potentially guiding more aggressive treatment strategies or patient selection for clinical trials. Importantly, therapeutic targeting of the GRPR–FAM135A–TENM3 axis may directly counteract PNI.

In conclusion, this study uncovers, for the first time, the neuro-oncological mechanisms underlying neural invasion in prostate cancer and identifies FAM135A as a pivotal driver of tumor nerve invasion. FAM135A is transcriptionally activated by the GRPR–MED1 axis, imported into the nucleus via RAN, and subsequently promotes TENM3 expression, facilitating neural invasion by tumor cells. These findings provide a novel framework for therapeutic targeting of the GRPR–FAM135A–TENM3 pathway to combat PNI and neural invasion in prostate cancer.

Materials and Methods

Patient samples

Prostate cancer tissue specimens were collected from patients undergoing surgical resection at Shanghai Ruijin Hospital. The presence of perineural invasion (PNI) was independently assessed by two experienced genitourinary pathologists. Cases were classified as PNI-

positive only when both pathologists confirmed tumor cells infiltrating the perineural space.

Analysis of public gene expression data

We utilized the transcriptomic dataset from Prueitt RL *et al*. [38] (GEO accession: GSE10779), which was generated using the Affymetrix Human Genome U133 Plus 2.0 Array. Raw CEL files were processed using the justRMA function of the affy R package, performing background correction and quantile normalization. Probes were mapped to gene symbols according to platform annotations. Differential expression between PNI-positive and PNI-negative tumors was determined using the limma package, with significance defined as |log2 fold change| > 1 and FDR-adjusted p-value < 0.05. Functional enrichment analyses for Gene Ontology (GO) and KEGG pathways were performed using clusterProfiler, with FDR < 0.05 considered significant.

Pathological evaluation of PNI

PNI was defined as tumor cells encasing at least one-third of a nerve circumference, following established urological pathology standards [55]. Two independent pathologists, blinded to molecular data, reviewed all specimens. Discrepancies were resolved via consensus under a multi-head microscope. To avoid misidentification of Schwann cells as tumor cells, dual immunohistochemical (IHC) staining for S100 was performed. Specimens were considered PNI-positive only if cytokeratin-positive tumor cells were clearly located within the perineural space and surrounded by S100-positive Schwann cells.

Immunohistochemistry (IHC)

Sections of paraffin-embedded tissue were subjected to dual IHC staining for FAM135A and S100 to distinguish tumor cells from Schwann cells. Slides were incubated overnight at 4°C with primary antibodies (Cell Signaling Technology, Danvers, USA), washed three times with PBS, and then incubated with biotin-conjugated secondary antibodies (Cell Signaling Technology) for 1 hour at room temperature. Visualization was performed with DAB (Sigma-Aldrich, St. Louis, USA) and counterstained with hematoxylin. Staining intensity was scored on a 0–3 scale (0 = negative, 1 = weak, 2 = moderate, 3 = strong). The proportion of positive cells was scored as 0 (<1%), 1 (1–25%), 2 (25–50%), 3 (50–75%), or 4 (>75%). The final IHC score was calculated as the product of intensity and proportion scores. PNI-positive classification required FAM135A-positive tumor cells within the perineural space surrounded by S100-positive Schwann cells.

Cell lines and culture

Human prostate cancer cell lines PC3 and DU145, rat pheochromocytoma PC-12, and human embryonic kidney 293T cells were obtained from ATCC. PC3, DU145, and PC-12 cells were cultured in RPMI-1640 supplemented with 10% fetal bovine serum (Gibco, Thermo Fisher Scientific) under standard conditions (37°C, 5% CO_2).

Stable lentiviral shRNA knockdown

FAM135A-targeting shRNA and control shRNA (shNC) were cloned into GV248 lentiviral vectors (Genechem, Shanghai, China). Prostate cancer cells were seeded at 1 × 10^4 cells per well in 24-well plates and transduced with 5 μL of lentiviral ps per well. After 8 hours, the medium was replaced with fresh complete medium. Cells were selected with puromycin for 3 weeks to generate stable knockdown lines.

Cell proliferation assay

Cells were plated in 96-well plates and incubated at 37°C in 5% CO_2. At 24, 48, and 72 hours, cell proliferation was assessed using the Cell Counting Kit-8 (CCK-8, Dojindo Molecular Technologies, Kyushu, Japan). CCK-8 solution was added to each well and incubated for 2 hours, after which absorbance at 450 nm was measured using a Bio-Rad microplate reader to quantify viable cell numbers.

Colony formation assay

To assess long-term proliferative capacity, cells in the logarithmic growth phase were harvested, counted, and resuspended in complete culture medium. Each experimental group was seeded at 500 cells per well in 6-well plates. Cultures were maintained for 14 days, or until colonies contained more than 50 cells. Medium was refreshed every 3 days, and cell morphology was monitored. Colonies were fixed with 4% paraformaldehyde for 15–30 minutes, followed by staining with 1 mL crystal violet (Sigma-Aldrich, St. Louis, USA) for 10–20 minutes. Excess dye was removed by PBS washes, and colony formation was documented via photography.

Flow cytometry for apoptosis (Annexin V-FITC/PI assay)

Apoptotic rates were determined using the Annexin V-FITC/PI kit (Beyotime Biotechnology, Shanghai, China). PC3 and DU145 cells were collected, washed with PBS, and resuspended in 500 µL binding buffer. Cells were incubated with 5 µL Annexin V-FITC/PI for 15 minutes at room temperature in the dark. Apoptotic populations were quantified using flow cytometry.

Transwell invasion assay

Transwell chambers were pre-coated with Matrigel (BD Biosciences, San Jose, CA, USA). 2×10^5 cells in serum-free medium were placed in the upper chamber, while the lower chamber contained medium supplemented with 20% FBS as a chemoattractant. After 48 hours of incubation, non-invading cells were removed from the upper surface. Invading cells on the lower surface were fixed with methanol, stained with crystal violet, and counted under a microscope in randomly selected fields, with experiments repeated in triplicate.

Wound healing assay

Cells were cultured to approximately 90% confluency in culture plates. A linear scratch was generated using a pipette tip, followed by one PBS wash to remove detached cells. Fresh medium was added, and wound closure was monitored and imaged at defined time points to assess migratory capacity.

Dorsal root ganglion (DRG) isolation

DRGs were dissected from the lumbar region of neonatal rats and digested sequentially with papain and collagenase. Dissociated DRG neurons were plated in 24-well plates and cultured in DMEM/F-12 medium (Gibco, Thermo Fisher Scientific) at 37°C with 5% CO_2 for 24 hours. Cytarabine (ara-C, 5 µg/mL) was then added for 24 hours to inhibit non-neuronal cell growth.

Tumor cell-DRG co-culture assay

Following established protocols, DRGs from 8-day-old Sprague-Dawley rats were positioned ~0.5 mm from clusters of prostate cancer cells within a growth-factor-reduced Matrigel matrix. Co-cultures were maintained in neurobasal medium (Invitrogen, Thermo Fisher Scientific) supplemented with 10% FBS, 100 U/mL penicillin, 100 µg/mL streptomycin, 0.5 mM L-glutamine, and 2% B-27. Medium was refreshed every 2 days, and after 48 hours, tumor migration towards DRGs was quantified as the nerve invasion index (α/γ), while DRG axon extension toward cancer cells was measured as the DRG outgrowth index (β/γ).

3D perineural invasion (PNI) model using PC-12 cells

PC-12 cells, differentiated with NGF to exhibit neuronal characteristics, were labeled with Cell-Tracker Green CMFDA (Invitrogen, Thermo Fisher Scientific) and embedded at 1×10^4 cells per 1.5 µL Matrigel supplemented with 75 µM forskolin (Sigma-Aldrich) in 6-well plates for 24 hours. Prostate cancer cells, stained with Cell-Tracker Red CMTPX, were added around the neuronal matrix and cultured for 48 hours. Cancer cell invasion into the neuronal network was visualized under a fluorescence microscope (Olympus Corporation, Tokyo, Japan).

Transwell-based PNI assay

A complementary PNI model was established using a Transwell system. Upper chambers were seeded with cancer cells, while PC-12 cells occupied the lower chambers. After 24 hours, non-migrating cells on the upper surface were removed. Invaded cancer cells on the lower membrane were stained with 0.1% crystal violet and imaged using an inverted microscope (DMR, Leica Microsystems, Wetzlar, Germany).

In vivo perineural invasion (PNI) model

To establish a PNI model in vivo, four-week-old nude mice were anesthetized with isoflurane (Sigma-Aldrich, St. Louis, MO, USA), and the right sciatic nerve was surgically exposed following published protocols [56, 57]. Prostate cancer cells (1×10^5 cells/µL) were injected in 5 µL volumes adjacent to the sciatic nerve using a 10 µL microsyringe under microscopic guidance. Mice were monitored weekly for tumor growth, body weight, sciatic nerve integrity, and limb motor function over a 7-week period. Sciatic nerve function was quantified using the toe spread distance between the first and fifth toes, and limb performance was scored on a scale from 4 (normal) to 1 (complete paralysis). All procedures were performed in compliance with ARRIVE guidelines.

RNA-sequencing and bioinformatic analysis

Total RNA was isolated from DU145 and PC-3 cells with or without PCDH12A knockdown using TRIzol reagent (Invitrogen, Thermo Fisher Scientific). Libraries were constructed for mRNA sequencing and sequenced, with raw data deposited appropriately. Differential gene expression analysis was conducted using DESeq2, and

genes with |log2 fold change| >1 and FDR-adjusted $p < 0.05$ were considered significant. Functional enrichment, including Gene Ontology (GO) and KEGG pathway analyses, was performed via the DAVID database, with $P < 0.05$ as the cutoff for significance.

Co-immunoprecipitation (Co-IP) and mass spectrometry (MS)

Cells expressing Flag-tagged FAM135A or empty vector were lysed, and lysates were incubated with Anti-Flag M2 Affinity Gel (Sigma-Aldrich). After thorough washing, bound proteins were eluted and subjected to trypsin digestion. Peptides were analyzed by LC-MS/MS, and data were searched against the SwissProt human protein database for identification.

Quantitative real-time PCR (qRT-PCR)

Total RNA extraction was performed using TRIzol reagent (Invitrogen, Thermo Fisher Scientific, Cat#15596026). RNA concentration and purity were measured using a NanoDrop spectrophotometer. One microgram of RNA was reverse-transcribed using PrimeScript RT Master Mix (TaKaRa, Cat# RR036A). qRT-PCR was conducted using TB Green Premix Ex Taq II (TaKaRa, Cat# RR820A) on a QuantStudio 5 Real-Time PCR System (Applied Biosystems) with cycling parameters: 95°C for 30 s, 95°C for 3 s, 60°C for 30 s, 40 cycles. Relative gene expression was calculated using the $2^{-}\Delta\Delta Ct$ method.

Western blotting

Cells were lysed in RIPA buffer (Beyotime Biotechnology, Shanghai, China), and protein concentration was quantified using the BCA assay (Thermo Fisher Scientific). Proteins were separated on 12% SDS-PAGE gels and transferred onto PVDF membranes (Millipore Sigma, Burlington, MA, USA). Membranes were blocked in 5% skim milk for 1 hour at room temperature and incubated with primary antibodies (Cell Signaling Technology, Danvers, USA) overnight at 4°C. After three washes with TBST, membranes were incubated with secondary antibodies (Cell Signaling Technology) for 1 hour, washed again, and visualized using ECL detection. Band intensities were quantified to determine relative protein levels.

Chromatin immunoprecipitation (ChIP-qPCR)

ChIP was performed using the BersinBio™ ChIP Kit (Catalog Bes5001, Guangzhou, China). Approximately 2×10^7 cells were fixed with 1% formaldehyde for 10 minutes, lysed, and chromatin was fragmented by sonication. Anti-STAT3 IgG (Cell Signaling Technology) was used to immunoprecipitate protein-DNA complexes. DNA was recovered after reversing cross-links, and ChIP-qPCR was performed using SYBR Green on the QuantStudio™ Dx Real-Time PCR Instrument (Thermo Fisher Scientific).

Hematoxylin and eosin (H&E) staining

Paraffin-embedded tissue sections were deparaffinized in xylene (Sigma-Aldrich) and dehydrated through graded ethanol. Sections were stained with hematoxylin for ~5 minutes, differentiated in hydrochloric acid-ethanol solution, rinsed with tap water, and counterstained with eosin. After dehydration and clearing in xylene, slides were cover-slipped with neutral resin and imaged under a light microscope.

Statistical analysis

Data are presented as mean ± SD. GraphPad Prism 8.2 (GraphPad Software, Inc.) was used for statistical comparisons. Unpaired Student's t-tests were applied for two-group comparisons. For experiments involving three groups, one-way ANOVA with Dunnett's post hoc test was employed to compare each group against the control. All tests were two-sided, and $P < 0.05$ was considered statistically significant.

Acknowledgments: None

Conflict of Interest: None

Financial Support: None

Ethics Statement: None

References

1. Siegel RL, Miller KD, Wagle NS, Jemal A. Cancer statistics, 2023. CA Cancer J Clin. 2023;73:17–48.
2. Rebello RJ, Oing C, Knudsen KE, Loeb S, Johnson DC, Reiter RE, et al. Prostate cancer. Nat Rev Dis Primers. 2021;7:9.
3. Desai K, McManus JM, Sharifi N. Hormonal therapy for prostate cancer. Endocr Rev. 2021;42:354–73.
4. Cheng Q, Butler W, Zhou Y, Zhang H, Tang L, Perkinson K, et al. Pre-existing castration-resistant

prostate cancer-like cells in primary prostate cancer promote resistance to hormonal therapy. Eur Urol. 2022;81:446–55.

5. Winkler F, Venkatesh HS, Amit M, Batchelor T, Demir IE, Deneen B, Gutmann DH, Hervey-Jumper S, Kuner T, Mabbott D, Platten M, Rolls A, Sloan EK, Wang TC, Wick W, Venkataramani V. Monje, cancer neuroscience: state of the field, emerging directions. Cell. 2023;186:1689–707.
6. Prillaman M. How cancer hijacks the nervous system to grow and spread. Nature. 2024;626:22–4.
7. Anastasaki C, Gao Y, Gutmann DH. Neurons as stromal drivers of nervous system cancer formation and progression. Dev Cell. 2023;58:81–93.
8. Pan C, Winkler F. Insights and opportunities at the crossroads of cancer and neuroscience. Nat Cell Biol. 2022;24:1454–60.
9. Keough MB, Monje M. Neural signaling in cancer. Annu Rev Neurosci. 2022;45:199–221.
10. Niu Y, Forster S, Muders M. The role of perineural invasion in prostate cancer and its prognostic significance. Cancers (Basel). 2022. https://doi.org/10.3390/cancers14174065.
11. Teramoto Y, Wang Y, Miyamoto H. Risk stratification by quantification of perineural cancer invasion on prostate needle core biopsy: should it be counted? J Urol. 2023;210:639–48.
12. Hou Y, Lin B, Xu T, Jiang J, Luo S, Chen W, et al. The neurotransmitter calcitonin gene-related peptide shapes an immunosuppressive microenvironment in medullary thyroid cancer. Nat Commun. 2024;15:5555.
13. Fu Y, Shen K, Wang H, Wang S, Wang X, Zhu L, et al. Alpha5 nicotine acetylcholine receptor subunit promotes intrahepatic cholangiocarcinoma metastasis. Signal Transduct Target Ther. 2024;9:63.
14. Cao Y, Ge X, Zhu X, Han Y, Wang P, Akakuru OU, et al. Transformable neuropeptide prodrug with tumor microenvironment responsiveness for tumor growth and metastasis inhibition of Triple-Negative breast cancer. Adv Sci. 2023;10:e2300545.
15. Padmanaban V, Keller I, Seltzer ES, Ostendorf BN, Kerner Z, Tavazoie SF. Neuronal substance P drives metastasis through an extracellular RNA-TLR7 axis. Nature. 2024;633:207–15.
16. Lu C, Mahajan A, Hong SH, Galli S, Zhu S, Tilan JU, Abualsaud N, Adnani M, Chung S, Elmansy N, Rodgers J, Rodriguez O, Albanese C, Wang H, Regan M, Zgonc V, Blancato J, Krawczyk E, Gallicano GI, Girgis M, Cheema A, Izycka-Swieszewska E, Cavalli LR, Pack SD, Kitlinska J. Hypoxia-activated neuropeptide Y/Y5 receptor/RhoA pathway triggers chromosomal instability and bone metastasis in ewing sarcoma. Nat Commun. 2022;13:2323.
17. Wang J, Wei J, Pu T, Zeng A, Karthikeyan V, Bechtold B, Vo K, Chen J, Lin TP, Chang AP, Corey E, Puhr M, Klocker H, Culig Z, Bland T, Wu BJ. Cholinergic signaling via muscarinic M1 receptor confers resistance to docetaxel in prostate cancer, cell reports. Medicine. 2024;5:101388.
18. Liu YN, Liu MK, Wen YC, Li CH, Yeh HL, Dung PVT, et al. Binding of interleukin-1 receptor antagonist to cholinergic receptor muscarinic 4 promotes immunosuppression and neuroendocrine differentiation in prostate cancer. Cancer Lett. 2024;598:217090.
19. Shi DD, Guo JA, Hoffman HI, Su J, Mino-Kenudson M, Barth JL, Schenkel JM, Loeffler JS, Shih HA, Hong TS, Wo JY, Aguirre AJ, Jacks T, Zheng L, Wen PY, Wang TC, Hwang WL. Therapeutic avenues for cancer neuroscience: translational frontiers and clinical opportunities. Lancet Oncol. 2022;23:e62–74.
20. Huang D, Alexander PB, Li QJ, Wang XF. GABAergic signaling beyond synapses: an emerging target for cancer therapy. Trends Cell Biol. 2023;33:403–12
21. Chen ZF. A neuropeptide code for itch. Nat Rev Neurosci. 2021;22:758–76.
22. Kanehisa K, Koga K, Maejima S, Shiraishi Y, Asai K, Shiratori-Hayashi M, et al. Neuronal pentraxin 2 is required for facilitating excitatory synaptic inputs onto spinal neurons involved in pruriceptive transmission in a model of chronic itch. Nat Commun. 2022;13:2367.
23. Sheahan TD, Warwick CA, Cui AY, Baranger DAA, Perry VJ, Smith KM, et al. Kappa opioids inhibit spinal output neurons to suppress itch. Sci Adv. 2024;10:eadp6038.
24. Li H, Chen X, Xu J, Zhu L, Li C, Sun X, et al. GRP/GRPR enhances alcohol-associated liver injury through the IRF1-mediated Caspase-1 inflammasome and NOX2-dependent ROS pathway. Hepatology. 2024;79:392–408.
25. Li C, Ma QY, Liu XQ, Li HD, Yu MJ, Xie SS, et al. Genetic and pharmacological inhibition of GRPR

protects against acute kidney injury via attenuating renal inflammation and necroptosis. Mol Ther. 2023;31:2734–54.
26. Goto F, Kiyama Y, Ogawa I, Okuno H, Ichise T, Ichise H, et al. Gastrin-releasing peptide regulates fear learning under stressed conditions via activation of the amygdalostriatal transition area. Mol Psychiatry. 2022;27(3):1694–703.
27. Kayalar O, Oztay F, Ongen HG. Gastrin-releasing peptide induces fibrotic response in MRC5s and proliferation in A549s, cell communication and signaling. CCS. 2020;18:96.
28. Peng S, Zhan Y, Zhang D, Ren L, Chen A, Chen ZF, et al. Structures of human gastrin-releasing peptide receptors bound to antagonist and agonist for cancer and itch therapy. Proc Natl Acad Sci U S A. 2023;120:e2216230120.
29. Chen L, Zhang J, Chi C, Che W, Dong G, Wang J, et al. Lower-grade gliomas surgery guided by GRPR-targeting PET/NIR dual-modality image probe: a prospective and single-arm clinical trial. Theranostics. 2024;14:819–29.
30. Wang W, Wu KJ, Vellaisamy K, Leung CH, Ma DL. Peptide-conjugated long-lived theranostic imaging for targeting GRPr in cancer and immune cells. Angew Chem Int Ed Engl. 2020;59:17897–902.
31. Duan H, Moradi F, Davidzon GA, Liang T, Song H, Loening AM, Vasanawala S, Srinivas S, Brooks JD, Hancock S, Iagaru A. (68)Ga-RM2 PET-MRI versus MRI alone for evaluation of patients with biochemical recurrence of prostate cancer: a single-centre, single-arm, phase 2/3 imaging trial, the lancet. Oncology. 2024;25:501–8.
32. Sollini M, Calais J, Chiti A, Emmett L, Fanti S, Fendler W, Herrmann K, Hope TA, Sartor O, Shuch B, Tagawa S, Hofman MS. Novel Radiopharmaceuticals and Future of Theranostics in Genitourinary Cancers, European urology. 2024.
33. Nisman B, Oleinikov K, Nechushtan H, Maimon O, Atlan K, Peled N, Gross D, Peretz T, Meirovitz A. Grozinsky-Glasberg, plasma Progastrin-Releasing peptide and chromogranin A assays for diagnosing and monitoring lung Well-Differentiated neuroendocrine tumors: A brief report. J Thorac Oncology: Official Publication Int Association Study Lung Cancer. 2023;18:369–76.
34. Bakker IL, Froberg AC, Busstra MB, Verzijlbergen JF, Konijnenberg M, van Leenders G, Schoots IG, de Blois E, van Weerden WM, Dalm SU, Maina T, Nock BA, de Jong M. GRPr antagonist (68)Ga-SB3 PET/CT imaging of primary prostate cancer in Therapy-Naive Patients, journal of nuclear medicine: official publication. Soc Nuclear Med. 2021;62:1517–23.
35. Schollhammer R, Robert G, Asselineau J, Yacoub M, Vimont D, Balamoutoff N, et al. Comparison of (68)Ga-PSMA-617 PET/CT and (68)Ga-RM2 PET/CT in patients with localized prostate cancer who are candidates for radical prostatectomy: a prospective, single-arm, single-center, phase II study. journal of nuclear medicine: official publication Soc Nuclear Med. 2023;64:379–85.
36. Xu J, Hu M, Gao Y, Wang Y, Yuan X, Yang Y, et al. LncRNA MIR17HG suppresses breast cancer proliferation and migration as CeRNA to target FAM135A by sponging miR-454-3p. Mol Biotechnol. 2023;65:2071–85.
37. Lou X, Ye Z, Xu X, Jiang M, Lu R, Jing D, et al. Establishment and characterization of the third non-functional human pancreatic neuroendocrine tumor cell line. Hum Cell. 2022;35:1248–61.
38. Prueitt RL, Yi M, Hudson RS, Wallace TA, Howe TM, Yfantis HG, et al. Expression of MicroRNAs and protein-coding genes associated with perineural invasion in prostate cancer. Prostate. 2008;68:1152–64.
39. Yang Y, Guo L, Chen L, Gong B, Jia D, Sun Q. Nuclear transport proteins: structure, function, and disease relevance. Signal Transduct Target Ther. 2023;8:425.
40. El-Tanani M, Nsairat H, Mishra V, Mishra Y, Aljabali AAA, Serrano-Aroca A, et al. Ran GTPase and its importance in cellular signaling and malignant phenotype. Int J Mol Sci. 2023. https://doi.org/10.3390/ijms24043065
41. Fukuchi J, Hiipakka RA, Kokontis JM, Hsu S, Ko AL, Fitzgerald ML, et al. Androgenic suppression of ATP-binding cassette transporter A1 expression in LNCaP human prostate cancer cells. Cancer Res. 2004;64:7682–5.
42. Lee BH, Taylor MG, Robinet P, Smith JD, Schweitzer J, Sehayek E, et al. Dysregulation of cholesterol homeostasis in human prostate cancer through loss of ABCA1. Cancer Res. 2013;73:1211–8.
43. Hiwatari M, Seki M, Matsuno R, Yoshida K, Nagasawa T, Sato-Otsubo A, et al. Novel TENM3-ALK fusion is an alternate mechanism for ALK

activation in neuroblastoma. Oncogene. 2022;41:2789–97.

44. Saidi A, Stallons TA, Wong AG, Torgue JJ, Society of Nuclear Medicine. Preclinical investigation of [(212)Pb]Pb-DOTAM-GRPR1 for peptide receptor radionuclide therapy in a prostate tumor model. J Nucl Med. 2024. https://doi.org/10.2967/jnumed.124.268101
45. Liu X, Wang Y, Tao T, Zeng L, Wang D, Wen Y, et al. GRPR/extracellular signal-regulated kinase and NPRA/extracellular signal-regulated kinase signaling pathways play a critical role in spinal transmission of chronic itch. J Invest Dermatol. 2021;141:863–73.
46. Jin F, Irshad S, Yu W, Belakavadi M, Chekmareva M, Ittmann MM, et al. ERK and AKT signaling drive MED1 overexpression in prostate cancer in association with elevated proliferation and tumorigenicity, molecular cancer research. MCR. 2013;11:736–47.
47. Liu Q, Ma Z, Cao Q, Zhao H, Guo Y, Liu T, et al. Perineural invasion-associated biomarkers for tumor development. Biomed Pharmacother. 2022;155:113691.
48. Yin L, Li J, Wang J, Pu T, Wei J, Li Q, et al. MAOA promotes prostate cancer cell perineural invasion through SEMA3C/PlexinA2/NRP1-cMET signaling. Oncogene. 2021;40:1362–74.
49. Harada N, Ohmori Y, Yamaji R, Higashimura Y, Okamoto K, Isohashi F, et al. ARA24/Ran enhances the androgen-dependent NH2- and COOH-terminal interaction of the androgen receptor. Biochem Biophys Res Commun. 2008;373:373–7.
50. Berns DS, DeNardo LA, Pederick DT, Luo L. Teneurin-3 controls topographic circuit assembly in the hippocampus. Nature. 2018;554:328–33.
51. Hunyara JL, Daly KM, Torres K, Yurgel ME, Komal R, Hattar S, et al. Teneurin-3 regulates the generation of non-image-forming visual circuitry and responsiveness to light in the suprachiasmatic nucleus. PLoS Biol. 2023;21:e3002412.
52. Li XC, Wang MY, Yang M, Dai HJ, Zhang BF, Wang W, et al. A mutational signature associated with alcohol consumption and prognostically significantly mutated driver genes in esophageal squamous cell carcinoma. Ann Oncol. 2018;29:938–44.
53. Zaret KS, Carroll JS. Pioneer transcription factors: establishing competence for gene expression. Genes Dev. 2011;25:2227–41.
54. Su N, Wang Y, Qian M, Deng M. Combinatorial regulation of transcription factors and microRNAs. BMC Syst Biol. 2010;4:150.
55. Lee JT, Lee S, Yun CJ, Jeon BJ, Kim JM, Ha HK, et al. Prediction of perineural invasion and its prognostic value in patients with prostate cancer. Korean J Urol. 2010;51:745–51.
56. Zheng S, Hu C, Lin Q, Li T, Li G, Tian Q, et al. Extracellular vesicle-packaged PIAT from cancer-associated fibroblasts drives neural remodeling by mediating m5C modification in pancreatic cancer mouse models. Sci Transl Med. 2024;16:eadi0178.
57. Zhang W, He R, Yang W, Zhang Y, Yuan Q, Wang J, et al. Autophagic Schwann cells promote perineural invasion mediated by the NGF/ATG7 paracrine pathway in pancreatic cancer. J Exp Clin Cancer Res. 2022;41:48.